Eur. Phys. J. B **16**, 403–410 (2000)

THE EUROPEAN PHYSICAL JOURNAL B

EDP Sciences

Magnetic susceptibility and electrical conductivity of Perylene radical cation salts

R. Desquiotz, M. Hofmann, and E. Dormann[a]

Physikalisches Institut, Universität Karlsruhe, Engesserstr. 7, 76128 Karlsruhe, Germany

Received 23 November 1999

Abstract. Conduction electron properties of the quasi-one-dimensional conductors $(PE)_2XF_6 \times 2/3$ THF, X = P, As and $(PE)_4(SbF_6)_3$ (PE = perylene, THF = tetrahydrofurane) were investigated by measuring magnetic susceptibility and microwave conductivity in the temperature range from 10 K to 300 K. For quantitative analysis of the measurements a microscopic model was developed.

PACS. 71.30.+h Metal-insulator transitions and other electronic transitions – 72.80.Le Polymers; organic compound (including organic semiconductors)

1 Introduction

Many quasi-one dimensional conductors show a metal-semiconductor transition of the Peierls type [1]. Due to electron-phonon coupling a condensed state is established which is characterized by [2]

1. a static lattice distortion along the conducting axis with wave number $2k_F$, coupled with
2. a $2k_F$ charge density wave (CDW) built up by the electrons near the Fermi level
3. an energy gap at the Fermi level.

In this work, the conduction electron properties of three Perylene radical cation salts were investigated by analyzing magnetic susceptibility and microwave conductivity in the temperature range from 10 K to 300 K. The Perylene (PE) salts $(PE)_2XF_6 \times 2/3$ THF (X = P or As; THF = tetrahydrofurane) and $(PE)_4(SbF_6)_3$ have the one-dimensional stacking of the planar Perylene radical cations and a 4:3 stoichiometry of Perylene cations and hexafluoride complex monoanions in common. They differ in the packing of additional molecules between the quasi-one dimensionally conducting Perylene stacks: In the SbF_6 compound only the anion chains are squeezed between the Perylene stacks; they show, however, considerable disorder [3,4]. In the Perylene salts PF_6 and AsF_6, the conducting PE-stack is additionally surrounded by neutral Perylene molecules and partially disordered THF solvent molecules [4–6]. The consequences of these structural differences are presented in this contribution.

[a] e-mail: edo@piobelix.physik.uni-karlsruhe.de

2 Experimental details and results

The details of crystal growth and experimental preparation of the systems have already been described in preceding papers [3,5]. The magnetic susceptibility was measured with a Quantum Design SQUID magnetometer (Fig. 1). The magnetic susceptibility is dominated by the highly anisotropic molecular diamagnetism [7]. Molecular reorientations as observed at the structural phase transitions of Perylene salts [6] lead thus to variations of the magnetic susceptibility for fixed single crystal orientation. In order to prevent corresponding artefacts in the derivation of the temperature dependence of the conduction electron contribution, the measurements were performed for a large number of crystals at statistical orientation. Longitudinal (= along the stack axis) and transverse microwave conductivity was measured for single crystals using the cavity-perturbation method [8] (Figs. 2, 3). At 10.2 GHz the reflection method and at 4.6 GHz, 9.3 GHz and 23.5 GHz a transmission set-up were used [9].

3 Theoretical description

3.1 Electronic density of states

First we have to introduce the required approximations and definitions. We will describe the organic quasi-1D conductors as interacting electron-phonon systems, *i.e.* we don't consider the electron-electron interaction. The latter usually leads to a significant enhancement of the Pauli spin susceptibility which is not observed in Perylene radical cation salts.

The usual starting-point for describing a one-dimensional metal with dominant electron-phonon

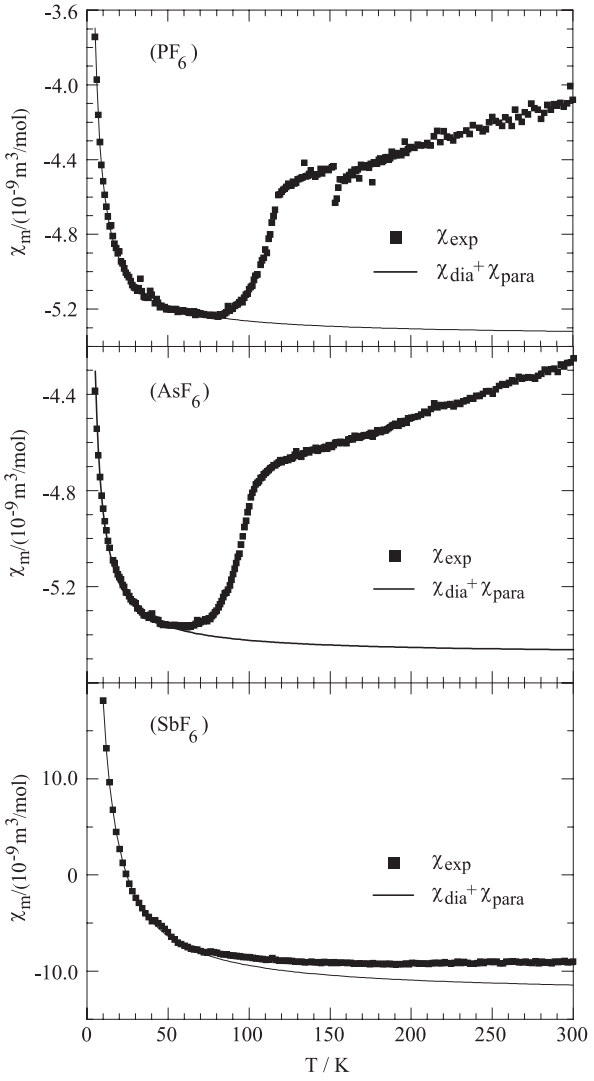

Fig. 1. Molar static magnetic susceptibility of $(PE)_2PF_6 \times 2/3$ THF, $(PE)_2AsF_6 \times 2/3$ THF and $(PE)_4(SbF_6)_3$ (SI-units). The solid line shows the fit of $\chi_{dia} + \chi_{para}$ obtained from the 2–50 K range (2–35 K for SbF_6).

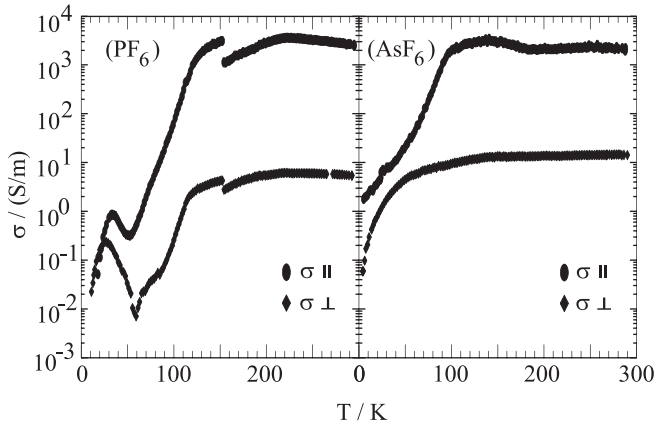

Fig. 2. Longitudinal and transverse microwave conductivity of $(PE)_2PF_6 \times 2/3$ THF and $(PE)_2AsF_6 \times 2/3$ THF.

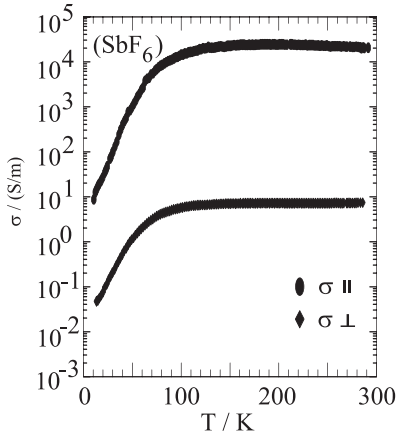

Fig. 3. Longitudinal and transverse microwave conductivity of $(PE)_4(SbF_6)_3$.

interaction is the 1D-Fröhlich Hamiltonian [10]

$$\hat{H} = \hat{H}_\mathrm{e} + \hat{H}_\mathrm{p} + \hat{H}_\mathrm{ep} \tag{1}$$

with

$$\hat{H}_\mathrm{e} = \sum_{k,s} \epsilon(k) \hat{c}^+_{k,s} \hat{c}_{k,s}$$

$$\hat{H}_\mathrm{p} = \sum_q \hbar\omega_q \left(\hat{b}^+_q \hat{b}_q + \frac{1}{2} \right)$$

$$\hat{H}_\mathrm{ep} = \sum_{k,s} \sum_q g(q) \hat{c}^+_{k+q,s} \hat{c}_{k,s} (\hat{b}^+_{-q} + \hat{b}_q)$$

$\hat{c}^+_{k,s}$ and $\hat{c}_{k,s}$ are electron creation and annihilation operators, $\hat{b}^+_q$ and $\hat{b}_q$ phonon operators. We don't consider spin-dependent interactions, thus $\sum_s = 2$.

As it is well known, one can treat this Hamiltonian in a mean field approximation. In this model, a Peierls transition occurs at a certain temperature T_MF. Below T_MF, a temperature-dependent band gap of $2\,|\langle \Delta \rangle|$ is opened at the Fermi level. $|\langle \Delta \rangle|$ is proportional to the amplitude of the lattice distortion at $q_0 = \pm 2k_\mathrm{F}$.

$$\langle \Delta \rangle = g(q_0) \left(\frac{\hbar}{2M\omega_{q_0}} \right)^{1/2} \left\langle \hat{b}_{q_0} + \hat{b}^+_{-q_0} \right\rangle . \tag{2}$$

A more accurate treatment of the problem leads to the conclusion that such a state is not stable in one-dimensional systems. As predicted by the Landau theorem, fluctuations of the order parameter $\langle \Delta \rangle$ destroy any long range order. That means $|\langle \Delta \rangle| = 0$ for $T > 0$, but the gap fluctuation $\langle |\Delta|^2 \rangle \neq 0$. To describe "real" Peierls systems one has to introduce an appropriate three-dimensional coupling. In such "quasi-one-dimensional conductors" a Peierls transition occurs at some temperature T_p with $0 < T_\mathrm{p} < T_\mathrm{MF}$ with the ratio $T_\mathrm{p}/T_\mathrm{MF}$ depending on the 3D-coupling [11].

Currently there exists no single model to describe real Peierls systems in the whole temperature range above and below the phase transition. Therefore one has to use different methods in the regions above and below T_p. As it is our aim to describe experimental curves, we will be satisfied with approximate or phenomenological solutions for the different temperature ranges.

High temperature region $\mathsf{T} \geq \mathsf{T_p}$

In the temperature range $T \geq T_\mathrm{p}$ we will use a method formerly introduced by Rice and Strässler [12] treating the electron-phonon interaction in second-order perturbation theory and adding a phononic interchain coupling, *i.e.* a dispersion of the phonons perpendicular to $\mathbf{q}_0$ (the chain direction).
For details of the calculation we refer to [12,13].

The renormalized phonon spectrum in the region of the soft mode $\mathbf{q}_0 = (0, 0, 2k_\mathrm{F})$ is then [11]

$$\Omega^2_{\mathbf{q}_0+\mathbf{P}} = \Omega^2_{\mathbf{q}_0}\left[1 + \xi^2_\parallel P^2_z\right] + \omega^2_{\mathbf{q}_0}\xi^2_\perp (P^2_x + P^2_y). \quad (3)$$

One can calculate the electron self energy as [12,14]

$$\Sigma(k, \mathrm{i}E_n) = -\frac{1}{\beta}\sum_{\mathrm{i}\hbar\omega_l}\sum_q |g(q)|^2\, \mathcal{G}^0(k-q, \mathrm{i}E_n - \mathrm{i}\hbar\omega_l) \times \mathcal{D}(q, \mathrm{i}\hbar\omega_l). \quad (4)$$

Gap fluctuation, correlation lengths and renormalized phonon frequency are related as

$$\left\langle |\Delta|^2 \right\rangle = \pi\hbar v_\mathrm{F}\frac{k_\mathrm{B}Ta_\perp}{2\xi_\parallel}\left(\frac{\Omega^2_{\mathbf{q}_0}}{\lambda\omega^2_{\mathbf{q}_0}} + 2\xi^2_\perp\right)^{-1/2} \quad (5)$$

with $a_\perp$ being the distance between neighbouring stacks.

The main problem is now to find values of the correlation lengths and the renormalized phonon frequency as functions of temperature. The best way should be to calculate these functions self-consistently which is barely possible. But there exist several approximations for different temperature regions. To get values of Ω_{2k_F} and $\xi_\parallel$ we use an approximation introduced by Patton and Sham [14] for the temperature range near T_p and the Ginzburg-Landau method of Scalapino *et al.* [15] around T_MF. In the intermediate temperature range we interpolate between the two limiting regions. The gap fluctuation is calculated *via* (5), the transverse correlation length is used as a fit parameter. The other fit parameter is the longitudinal electron-phonon coupling constant $g(2k_\mathrm{F})$, respectively its dimensionless version

$$\lambda = \frac{D_0}{\omega^2_{2k_\mathrm{F}}}|g(2k_\mathrm{F})|^2 \quad (6)$$

which determines T_MF and the zero-temperature gap value $|\langle\Delta\rangle|_{T=0}$.

Low temperature region $\mathsf{T} < \mathsf{T_p}$

Below the transition temperature T_p three-dimensional long range order is established. This state is characterized by the non-zero expectation value $|\langle\Delta\rangle|$ of the order parameter. Therefore, an appropriate description is to use the mean field Hamiltonian again, just with a modified temperature dependence of $|\langle\Delta\rangle|$. Schulz [11,16] has introduced the so-called scaled mean field gap equation

$$1 = \frac{\lambda}{2}\int_{-\epsilon_\mathrm{B}}^{\epsilon_\mathrm{B}} \frac{1}{\sqrt{\epsilon^2 + |\langle\Delta\rangle|^2}} \tanh\left[\frac{\sqrt{\epsilon^2 + |\langle\Delta\rangle|^2}}{2k_\mathrm{B}T^*}\right] \mathrm{d}\epsilon \quad (7)$$

with

$$T^* = T\frac{T_\mathrm{p}}{T_\mathrm{MF}}\,. \quad (8)$$

From equation (7) the temperature dependence of $|\langle\Delta\rangle|$ is obtained. Then the density of states of the upper subband is just

$$D^+(\epsilon^+) = D_0\frac{\epsilon^+}{\sqrt{(\epsilon^+)^2 - |\langle\Delta\rangle|^2}} \quad (9)$$

with

$$\epsilon^+ = \sqrt{\epsilon^2 + |\langle\Delta\rangle|^2}. \quad (10)$$

3.2 Crystal parameters and band structure

Band structure calculations for $(\mathrm{PE})_2\mathrm{PF}_6 \times 2/3$ THF and $(\mathrm{PE})_4(\mathrm{SbF}_6)_3$ were performed by Whangbo and coworkers [17]. For the following analysis, we use a simple linear dispersion for the one-dimensional band structure around the Fermi level in the metallic (undisturbed) state:

$$\epsilon(k) = \begin{cases} \hbar v_\mathrm{F}(k - k_\mathrm{F}) & \text{for } |k - k_\mathrm{F}| < \delta_\mathrm{B} \\ -\hbar v_\mathrm{F}(k + k_\mathrm{F}) & \text{for } |k + k_\mathrm{F}| < \delta_\mathrm{B} \end{cases} \quad (11)$$

with Fermi velocity v_F and wave vector k_F. Values for the Fermi velocity were obtained from the band structure calculations and were confirmed (for $(\mathrm{PE})_2\mathrm{PF}_6 \times 2/3$ THF) by measurements of optical reflectivity [13] (see Tab. 1).

3.3 Conduction electron susceptibility

The magnetic susceptibility of the conduction electrons is directly obtained from the density of states. We use the molar susceptibility

$$\chi^{\mathrm{c.e.}}_\mathrm{m} = N_\mathrm{A}c\frac{y}{x}\mu_0\mu^2_\mathrm{B}\int D(\epsilon)\left(-\frac{\partial f}{\partial\epsilon}\right)\mathrm{d}\epsilon \quad (12)$$

where N_A is the Avogadro constant, c the lattice constant in chain direction, x the number of formula units in one elementary cell and y the number of chains per unit area. For D one has to use the density of states per energy and volume, including a factor of 2 for both spin directions.

Table 1. Table of the numerical results

	$(PE)_2PF_6 \times 2/3$ THF	$(PE)_2AsF_6 \times 2/3$ THF	$(PE)_4(SbF_6)_3$
Band structure calculations			
v_F / (10^5 m/s)	1.63	1.63	1.74
$\chi_0(300\,K)$ / (10^{-9} m^3/mol)	1.25	1.25	3.73
Susceptibility measurements			
C / (10^{-9} m^{3}K/mol)	8.26 ± 0.76	5.90 ± 0.39	(3.05 ± 0.37) $\times 10^2$
χ_{Dia} / (10^{-9} m^3/mol)	−5.35± 0.21	−5.48 ± 0.13	−12.5 ± 1.1
T_p / K	118 ± 2	102 ± 2	-
Model calculations for $\chi_{c.e.}$			
λ	0.56	0.54	0.35
T_{MF} / K	273	253	330
$\langle\Delta\rangle\,(T=0)$ / meV	41	38	-
Model calculations for σ			
$\mu_{ges}(250\ K)$ / (10^{-4} m^2/Vs)	2.5	1.5	11.5
$\tau_\perp(250\,K)$ / 10^{-11} s	13.6	6.0	20.5

3.4 Conductivity

Semiclassical theory

It is rather difficult to include all aspects of transport behaviour of Peierls systems in one single model, especially at the level of quantum microscopic theory. Existing models focus on certain properties of such systems, for example CDW transport (see for example [18] and references therein). We are mostly interested in the conductivity due to single electrons, and to treat this problem in an economic way, we will rest on the basic level of semiclassical theory.

The conductivity of a quasi-one dimensional system is then calculated with the Boltzmann equation and reads (with N_c the number of chains per unit area)

$$\sigma = 2N_c e^2 \int |v(\epsilon)|^2 \tau(\epsilon) \left(-\frac{\partial f}{\partial \epsilon}\right) D(\epsilon) \mathrm{d}\epsilon. \qquad (13)$$

The situation is quite clear in the low temperature (semiconducting state) and the high temperature (metallic state) limits, where a well defined band structure can be used. For the fluctuation regime there exist two possibilities.

First, we can treat the lattice fluctuations as an additional scattering potential. This will be correct as long as the mean free path $\bar{l}$ of the electrons is long enough to use the Boltzmann equation. Furthermore, the longitudinal correlation length $\xi_\parallel$ of the fluctuating lattice distortion must remain small. If $\bar{l} < \xi_\parallel$ the electrons will rather "see" a local gap than a scattering potential.

For the temperature region approaching T_p one may use the method first introduced by Johnston [19]. In this model the influence of fluctuations is summarized in an effective (temperature-dependent) electronic gap Δ_{eff}. This is a phenomenological treatment, but it has two advantages. First of all, one can describe the different temperature regions with one and the same tool. And second – what is more important in our case – it is possible to derive an effective mobility without knowing details of the scattering mechanisms in the crystal. Therefore this method is used in the following. For a detailed discussion of the scattering processes and the intrinsic transport quantities we refer to [13].

3.5 Analysis procedure

The combined analysis of magnetic susceptibility and conductivity is performed in several steps. The procedure is described in detail in [13].

By combining results from EPR analysis and static susceptibility measurements, all contributions to the static magnetic susceptibility can be separated. Because no magnetic ordering is observed, the susceptibility has only three contributions: the diamagnetic and paramagnetic susceptibility of the bounded electrons and the conduction electron susceptibility.

$$\chi = \chi_{dia} + \chi_{para} + \chi_{c.e.}. \qquad (14)$$

The paramagnetic contribution obeys a Curie law and is determined by the concentration of impurities and structural defects with localized magnetic moments.

The susceptibility of the conduction electrons was then analyzed with the models described in Section 3 and [13]. In cases where a Peierls transition occurred, the relevant parameters as transition temperature T_p, energy gap $|\langle\Delta\rangle|$, longitudinal electron-phonon coupling λ and transverse correlation length $\xi_\perp$ were determined.

To analyze the conductivity measurements, the effective electron density in the upper partial band $\bar{n}$ and effective density of states $\bar{D}$ were calculated from the conduction electron susceptibility results [13]. This allows the average mobility μ (in stack direction) and the transverse hopping time $\tau_\perp$ to be obtained from the conductivity results with

$$\sigma_\parallel = 2\bar{n}e\mu \qquad (15)$$

$$\sigma_\perp = \bar{D}\frac{e^2 a_\perp^2}{\tau_\perp} \qquad (16)$$

where $a_\perp$ is the distance between neighbouring stacks.

In the following, our discussion of the temperature-dependence always starts at room temperature and goes on towards lower temperatures.

4 Discussion of the results

4.1 Magnetic susceptibility, Peierls transition and electron-phonon-coupling

Magnetic susceptibility and EPR measurements on $(PE)_2PF_6 \times 2/3$ THF and $(PE)_2AsF_6 \times 2/3$ THF showed the absence of magnetic order in these systems [20,21]. The Curie paramagnetism dominates at low temperatures. Results for the Curie constant and the diamagnetism derived from Figure 1 are given in Table 1. The measured values for the diamagnetism are in good agreement with the theoretical ones. The concentration of spin 1/2 impurities is in the range of $1 \ldots 2 \times 10^{-3}$ per formula unit. The conduction electron susceptibility (Fig. 4) decreases with decreasing temperature throughout the temperature range analyzed, *i.e.* the systems are never in a pure metallic state.

For $(PE)_2PF_6 \times 2/3$ THF the step at (151 ± 2) K indicates a structural phase transition [6]. At $T_p = (118 \pm 2)$ K the Peierls transition occurs, and the susceptibility shows an activated behaviour below T_p. A more profound analysis with the models of Section 3 leads to the following results. As the structural phase transitions do not affect the relations in stack direction [4,6], the longitudinal electron-phonon coupling λ does not change above T_p. Values of about 0.5 indicate intermediate coupling. The mean field temperatures calculated from λ lie near room temperature, indicating that lattice fluctuations are still present in this temperature range. The transverse coupling is weak for high temperatures. In $(PE)_2PF_6 \times 2/3$ THF the transverse coupling increases abruptly below 151 K due to the structural phase transition. Towards the Peierls transition temperature the transverse correlation length increases as three-dimensional order is established. The analysis in Figure 4 gives $\lambda = 0.56$ and $T_{MF} = 273$ K. This agrees with the general temperature dependence of $\chi_{c.e.}$, indicating lattice fluctuations up to room temperature.

In $(PE)_2AsF_6 \times 2/3$ THF (Figs. 1 and 4) the structural phase transition is of a second-order nature [6], leading to a continuously increasing transverse phonon coupling from 170 K to 130 K. The Peierls transition occurs at $T_c = (102 \pm 2)$ K and is less sharp than in the PF_6 salt. The analysis of Figure 4 gives $\lambda = 0.54$ and $T_{MF} = 253$ K.

For $(PE)_4(SbF_6)_3$ the situation is different. First of all, the concentration of impurities is significantly higher than in the other systems (Fig. 1). That means, the paramagnetic contribution dominates to such an extent that it hides the conduction electron susceptibility. Therefore, additional EPR analysis was used to identify the different contributions and to fix the absolute values of the conduction electron susceptibility [3]. As shown in Figure 4, $\chi_{c.e.}$ decreases steadily towards lower temperatures without showing anomalies. There is no indication of phase transitions.

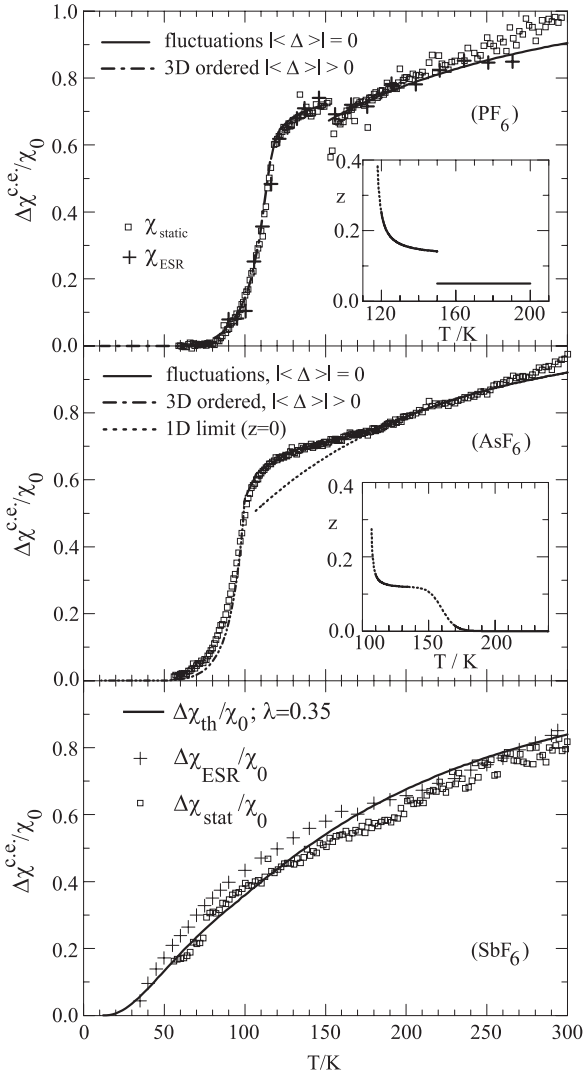

Fig. 4. Normalized conduction electron susceptibility of $(PE)_2PF_6 \times 2/3$ THF, $(PE)_2AsF_6 \times 2/3$ THF and $(PE)_4(SbF_6)_3$ compared to the results of the model calculation. $T = 130$ K was used for the normalization of the ESR-susceptibility for PF_6. Inset: $z = \xi_\perp / a_\perp$ is the transverse correlation length in units of the interstack distance.

$(PE)_4(SbF_6)_3$ fulfills the phenomenological conditions – anisotropic conductivity (Fig. 3) and suitable crystal structure [3] – for a one-dimensional conductor as well as the other two systems. Nevertheless $(PE)_4(SbF_6)_3$ undergoes no Peierls transition. So one can assume that lattice fluctuations suppress the Peierls transition in the whole temperature region in discussion. *A priori* there are two possible reasons for this – either lack of three-dimensional coupling or impurity effects. The detailed structural analysis points to the influence of anion-chain disorder [3].

For the quantitative analysis of the temperature dependence of the conduction electron magnetic susceptibility of $(PE)_4(SbF_6)_3$ in Figure 4 the one-dimensional limit of the model from Section 3 was used. The results of the numerical analysis are $\lambda = 0.35$ and $T_{MF} = 330$ K (Tab. 1).

4.2 Microwave conductivity

Figures 2 and 3 show the longitudinal and transverse microwave conductivity of the three systems. The absolute values of $\sigma_{\|}$ are rather low, lying in the range of 1.2×10^4 S/m at room temperature. The transverse conductivity is three orders of magnitude smaller than $\sigma_{\|}$, so all systems are proved to be quasi one-dimensional conductors.

The low absolute values result from the domain-like structure of the crystals, first shown by measurements of the diffusion constant with pulsed EPR [22]. The electron mobility therefore has two contributions, an intrinsic one caused by electron scattering due to lattice fluctuations and ordinary phonons, and a macroscopic or quasi-microscopic part due to the domain walls. This also explains why the longitudinal conductivity in $(PE)_2PF_6 \times 2/3$ THF and $(PE)_2AsF_6 \times 2/3$ THF increases with increasing microwave frequency [13,8]. It is important to mention that no difference was observed between the temperature dependence of the spin diffusion constant and microwave conductivity parallel to the stacking direction [23], proving that Peierls systems really are analyzed here.

The temperature dependence of $\sigma_{\|}$ in $(PE)_2PF_6 \times 2/3$ THF reflects a strong influence of the structural phase transitions. At 213 K the crystal splits up in two kinds of domains where the stack molecules are turned in different directions. This leads to additional electron scattering and therefore to a decrease of $\sigma_{\|}$ towards lower temperatures. At 151 K the stack molecule rotation forces the anions to move out of their original positions (or the other way around!) [6]. Therefore each second stack has to turn back a little bit, resulting in a doubling of the elementary cell in a direction. This is indicated by a step in the conductivity with higher values below the transition temperature. As the conduction electron susceptibility also steps to higher values below 151 K, this cannot be a band structure (band width) effect. It is more likely that the increase of the transverse coupling partly suppresses the lattice fluctuations, leading to reduced electron scattering.

The opening gap at the Peierls transition (118 K) results in an activated behaviour of the conductivity. The local maximum at 30 K indicates excitation of charge density waves, as a similar effect was not measured in the DC conductivity [24,25].

$(PE)_2AsF_6 \times 2/3$ THF shows a similar behaviour as $(PE)_2PF_6 \times 2/3$ THF, but the effects due to the structural phase transitions are less significant (Fig. 2). In this system the structure changes continuously [6,13] so that the effect on the conductivity can hardly be distinguished.

The microwave conductivity of $(PE)_4(SbF_6)_3$ gives no hints of phase transitions (Fig. 3), in agreement with the susceptibility results. Unlike the other systems, the conductivity is not frequency-dependent within the used frequency range (4.6 to 23 GHz). This might be due to a different domain size distribution than in the other systems [3,8,13].

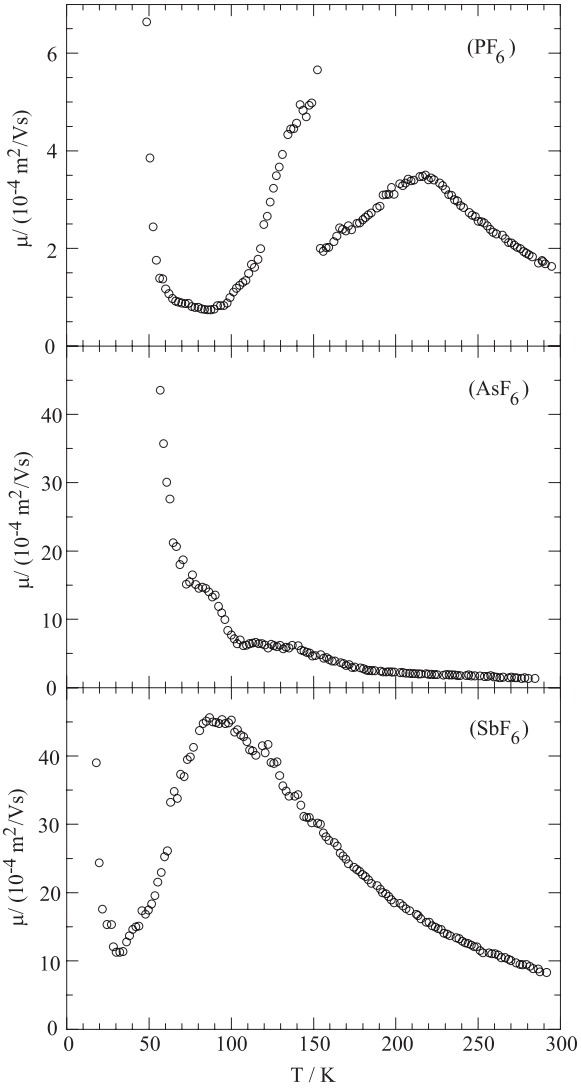

Fig. 5. Electron mobility in stack direction of $(PE)_2PF_6 \times 2/3$ THF, $(PE)_2AsF_6 \times 2/3$ THF and $(PE)_4(SbF_6)_3$.

4.3 Electron mobility and interchain hopping

Using the conductivity data for both orientations and the results from the susceptibility analysis, the average mobility in stack direction and the average transverse hopping time can be calculated, as reported in Section 3.

In order to derive the average mobility, plotted in Figure 5, the effective electron concentration

$$\overline{n} = \int_{+} D(\epsilon) f(\epsilon) \mathrm{d}\epsilon \tag{17}$$

is inserted in equation (15). Like the microwave conductivity parallel to the stacking direction, this average mobility reflects the influence of quasi-microscopic defects as well as the intrinsic variation. Actually, for all three compounds the intrinsic scattering rates are only of low importance for the total average scattering rates [13]. The influence of the structural phase transitions of the PF_6

salt at 213 K and 151 K and the dramatic increase of the average mobility due to the contribution of charge density waves at low temperatures can be seen in Figure 5. Typically, for all three Perylene salts, around room temperature the mobility increases with decreasing temperature, starting from similar values of about 1.5 cm^2/Vs for the PF_6 and AsF_6 salts, but a larger value of about 8 cm^2/Vs for the SbF_6 salt. Generally, a maximum of the mobility is reached in the "metallic" range around 90–150 K, followed by a decrease due to activated conductivity at lower temperatures, clearly visible for the PF_6 and SbF_6 salts. For the AsF_6 salt, the low-temperature minimum of the average mobility is covered by its more pronounced CDW contribution rising at $T_p = 102$ K already.

Using the integrated density of states

$$\overline{D} = \int D(\epsilon)(-\frac{\partial f}{\partial \epsilon})\mathrm{d}\epsilon \tag{18}$$

and the experimental results for $\sigma_\perp$ (Figs. 2, 3) the transversal hopping time $\tau_\perp$ is derived with equation (16). Since (due to the huge anisotropy of σ) the absolute value and temperature dependence of $\sigma_\perp$ depends critically on the precision of the single crystal orientation during the conductivity measurements, the influence of $\sigma_\parallel$ on the data analysis can not absolutely be excluded. Indeed, the $\tau_\perp$ values shown in Figure 6 for the "metallic" phase range in the order of magnitude of $0.5 \ldots 4 \times 10^4\, \bar{\tau}_\parallel$! The decrease of $\tau_\perp$ at the lowest temperatures is not an intrinsic effect, but seems to originate from the interplay of charge density wave excitations. Being roughly inversely proportional to the mobility, the transversal hopping time decreases with decreasing temperature for all three compounds starting at room temperature, but increases again at temperatures below 150–100 K as expected for phonon assisted hopping. It is important to note that for all temperatures between 300 K and 100 K the absolute values of the transversal hopping times of the three different Perylene salts agree within a factor of three and vary with temperature by less than 50% only.

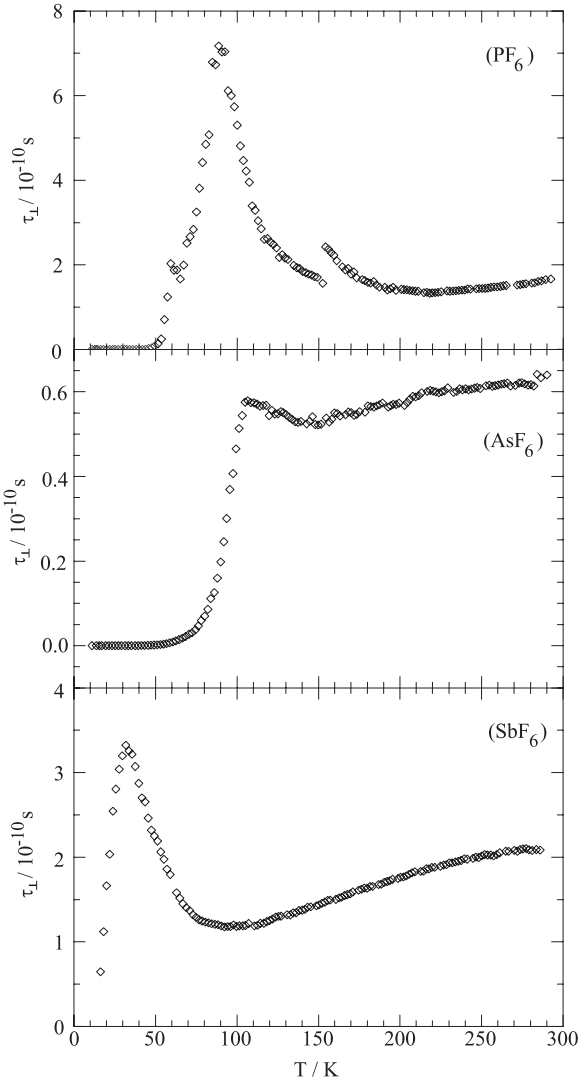

Fig. 6. Transverse hopping time of $(PE)_2PF_6 \times 2/3$ THF, $(PE)_2AsF_6 \times 2/3$ THF and $(PE)_4(SbF_6)_3$.

5 Conclusions

5.1 Structural phase transitions and Peierls transition in $(PE)_2PF_6 \times 2/3$ THF and $(PE)_2AsF_6 \times 2/3$ THF

A model of the structural phase transitions in $(PE)_2PF_6 \times 2/3$ THF was proposed in [6], considering the X-ray structural and EPR measurements. At 213 K the crystal splits up in two kinds of domains where the stack molecules are turned in different directions. The rotation angle increases with decreasing temperature. At 151 K the stack molecule rotation forces the anions to move out of their original positions. Therefore each second stack has to turn back a little bit, resulting in a doubling of the elementary cell in the *a*-direction. Only in this low temperature range, the anion rotational motion is frozen-in according to nuclear spin lattice relaxation analysis [26].

Applying this model to the susceptibility and conductivity results leads to the following conclusions. The rotation of the stack molecules below 213 K influences neither the one-dimensional conduction band nor the transverse coupling, as $\chi_{c.e}$ is not affected at all. The only anomaly of $\chi_{c.e}$ occurs at 151 K and was interpreted as a change of the transverse coupling due to the shift of the anions out of their original positions. If we further take into account that the absence of long-range order of the anion chains of $(PE)_4(SbF_6)_3$ perpendicular to the stack direction suppresses the Peierls transition in that system [3], we conclude that the Peierls transition in the PF_6- and AsF_6-systems is triggered by three-dimensional phonon coupling *via* the anions (*a*-direction). The structural measurements in both systems gave indications that there is an additional Coulomb interaction between the charge density waves at low temperatures in the *b*-direction however [6].

5.2 Behaviour of $(PE)_4(SbF_6)_3$

A naive explanation for the absence of a Peierls transition in $(PE)_4(SbF_6)_3$ would be based on impurity effects in the one-dimensional PE-stack. But several experimental results do not match with this assumption. First of all, the resistivity in $(PE)_4(SbF_6)_3$ and the fluctuation gap magnitude are not significantly higher than in the other systems. Furthermore, the EPR results suggest that most impurities are located on the surface of the crystal and do not get in contact with the conduction electrons [3]. This leads to the conclusion that the transverse coupling itself is suppressed. From crystal structure analysis it is known that the anion chains in $(PE)_4(SbF_6)_3$ have no long-range order in the *a*- and *b*-directions [3]. The related correlation length lies in the range of 400 Å, which is much less than extensions of several μm in the two other systems. If we assume that the ordered anions are needed for transverse phononic coupling, as was shown for the PF_6- and AsF_6-systems, this easily explains the lack of transverse coupling and suppression of the Peierls transition in $(PE)_4(SbF_6)_3$.

We thank I. Odenwald for crystal growth, M.T. Kelemen for the susceptibility measurements, and R. von Baltz, W. Brütting and D. Schweitzer for helpful discussions. This work was supported by the Deutsche Forschungsgemeinschaft within SFB 195 (Universität Karlsruhe (TH)).

References

1. R. Peierls, *Quantum Theory of Solids* (Oxford University Press, 1955).
2. S. Kagoshima, H. Nagasawa, T. Sambongi, *One-Dimensional Conductors* (Springer-Verlag, Berlin, 1988).
3. C. Buschhaus, R. Desquiotz, K. Eichhorn, M. Hofmann, K. Hümmer, V. Illich, M. Kelemen, S. Tarragona Auga, T. Wokrina, A. Zitsch, E. Dormann, Eur. Phys. J. B **8**, 57 (1999).
4. C. Buschhaus, E. Dormann, K. Eichhorn, K. Hümmer, R. Moret, S. Ravy, Synth. Metals **102**, 1757 (1999).
5. M. Burggraf, H. Dragan, P. Gruner-Bauer, H.W. Helberg, W.F. Kuhs, G. Mattern, D. Müller, W. Wendl, A. Wolter, E. Dormann, Z. Phys. B **96**, 439 (1995).
6. C. Buschhaus, R. Moret, S. Ravy, E. Dormann, Synth. Metals **108**, 21 (2000).
7. E. Dormann, Synth. Metals **27**, B 529 (1988).
8. M. Hofmann, diploma thesis, Universität Karlsruhe (TH), (unpublished), 1997.
9. G. Schaumburg, H.W. Helberg, J. Phys. III France **4**, 917 (1994).
10. M.J. Rice, S. Strässler, Solid State Comm. **13**, 125 (1973).
11. H.J. Schulz, in *Low-Dimensional Conductors and Superconductors (NATO ASI Series B Vol. 155)*, edited by D. Jérome, L.G. Caron (Plenum Press, New York, 1987).
12. M.J. Rice, S. Strässler, Solid State Commun. **13**, 1389 (1973).
13. R. Desquiotz, Ph.D. thesis (Shaker Verlag, Aachen, 1998).
14. L.J. Sham, *Pertubation approach to lattice displacements, in*: *Highly Conducting One-Dimensional Solids*, edited by J.T. Devreese, R.P. Evrard, V.E. van Doren (Plenum Press, New York, 1979).
15. D.J. Scalapino, M. Sears, R.A. Ferrell, Phys. Rev. B **6**, 3409 (1972).
16. D. Jérome, H.J. Schulz, Adv. Phys. **31**, 299 (1982).
17. M.-H. Whangbo, private communication.
18. G. Grüner: *Density Waves in Solids* (Addison-Wesley, Reading Massachusetts, 1994).
19. D.C. Johnston, Phys. Rev. Lett. **52**, 2049 (1984).
20. A. Wolter, M. Burggraf, H. Dragan, U. Fasol, E. Dormann, H.W. Helberg, D. Müller, Synth. Metals **71**, 1957 (1995).
21. U. Fasol, E. Dormann, Phys. Lett. A **222**, 281 (1996).
22. T. Wokrina, E. Dormann, N. Kaplan, Phys. Rev. B **54**, 10492 (1996).
23. T. Tashma, G. Alexandrowicz, N. Kaplan, E. Dormann, A.Grayevsky, A. Gabay, Synth. Metals **106**, 151 (1999).
24. W. Brütting, Ph.D. thesis, Universität Bayreuth, unpublished (1995).
25. W. Brütting, W. Rieß, Acta Phys. Polonica **87**, 852 (1995).
26. G. Nemec, V. Illich, E. Dormann, Synth. Metals **95**, 149 (1998).